Neuro-Oncology

19(7), 951–964, 2017 | doi:10.1093/neuonc/now297 | Advance Access date 28 February 2017

VDAC1 is a molecular target in glioblastoma, with its depletion leading to reprogrammed metabolism and reversed oncogenic properties

Tasleem Arif,* Yakov Krelin,* Itay Nakdimon, Daniel Benharroch, Avijit Paul, Daniela Dadon-Klein, and Varda Shoshan-Barmatz

Department of Life Sciences, and the National Institute for Biotechnology in the Negev, Ben-Gurion University of the Negev, Beer-Sheva, Israel (T.A., Y.K., I.N., A.P., D.D-K., V.S.-B.); Department of Pathology, Soroka University Medical Centre, and Faculty of Health Sciences, Ben-Gurion University of the Negev, Beer-Sheva, Israel (D.B.)

Corresponding Author: Dr Varda Shoshan-Barmatz, PhD, Department of Life Sciences, Ben-Gurion University, Beer Sheva, 84105, Israel (vardasb@bgu.ac.il).

*First co-authors.

Abstract

Background. Glioblastoma (GBM), an aggressive brain tumor with frequent relapses and a high mortality, still awaits an effective treatment. Like many cancers, GBM cells acquire oncogenic properties, including metabolic reprogramming, vital for growth. As such, tumor metabolism is an emerging avenue for cancer therapy. One relevant target is the voltage-dependent anion channel 1 (VDAC1), a mitochondrial protein controlling cell energy and metabolic homeostasis.

Methods. We used VDAC1-specific short interfering (si)RNA (si-VDAC1) to treat GBM cell lines and subcutaneous or intracranial-orthotopic GBM xenograft mouse models. Tumors were monitored using MRI, immunohistochemistry, immunoblotting, immunofluorescence, quantitative real-time PCR, transcription factor expression, and DNA microarray analyses.

Results. Silencing VDAC1 expression using si-VDAC1 in 9 glioblastoma-related cell lines, including patient-derived cells, led to marked decreases in VDAC1 levels and cell growth. Using si-VDAC1 in subcutaneous or intracranial-orthotopic GBM models inhibited tumor growth and reversed oncogenic properties, such as reprogrammed metabolism, stemness, angiogenesis, epithelial-mesenchymal transition, and invasiveness. In cells in culture, si-VDAC1 inhibits cancer neurosphere formation and, in tumors, targeted cancer stem cells, leading to their differentiation into neuronal-like cells. These VDAC1 depletion-mediated effects involved alterations in transcription factors regulating signaling pathways associated with cancer hallmarks.

Conclusion. VDAC1 offers a target for GBM treatment, allowing for attacks on the interplay between metabolism and oncogenic signaling networks, leading to tumor cell differentiation into neuron- and astrocyte-like cells. Simultaneously attacking all of these processes, VDAC1 depletion overcame GBM heterogeneity and can replace several anticancer drugs that separately target angiogenesis, proliferation, or metabolism.

Key words

glioblastoma | metabolism | mitochondria | siRNA | voltage-dependent anion channel

Glioblastoma (GBM) is the most common and aggressive malignant primary brain tumor and is associated with high rates of morbidity, relapse, and mortality.[1] GBM is a heterogeneous cancer, with tumors containing niches enriched for transiently quiescent and self-renewing cells that are essentially GBM cancer stem cells (GSCs).[2,3] Such intratumoral heterogeneity underlies the inability of conventional and targeted therapies to achieve long-term remission.[4] Cancer

Importance of the study

Here, we present a new concept of cancer cell metabolism modulation based on VDAC1 depletion using specific siRNA to reverse glioblastoma cell energy and metabolic reprogramming. As the mitochondria gatekeeper and a convergence point for various cell survival and death signals, VDAC1 acts at a "bottleneck" position, controlling metabolic homeostasis and apoptosis. We showed that VDAC1 depletion resulted in a multipronged attack on cancer hallmarks, reversing oncogenic properties via a reversal of cancer-reprogrammed metabolism, resulting in inhibited cell proliferation, tumor growth, invasiveness, and angiogenesis. VDAC1 depletion also targeted cancer stem cells, leading to their differentiation into neuronal-like cells. We thus explored metabolism, controlled by VDAC1, as an emerging target for controlling cancer cell reprogramming, and demonstrated the intricate interplay between metabolism and the oncogenic signaling network, with si-human VDAC1 representing an innovative and potent therapeutic strategy for glioblastoma and other cancers.

cells acquire a common set of properties, including high proliferation, resistance to apoptosis, and metabolic reprogramming, such as enhanced aerobic glycolysis (Warburg effect).[5,6] As such, cancer cells upregulate the transcription of genes related to glycolysis. Mitochondria play a role in reprogramming cellular metabolism,[7] with metabolic flexibility serving to balance tumor cell energy needs with requirements for metabolites and precursors.[6,8] Metabolic reprogramming in GBM and its influence on epigenetics were recently reviewed.[9] Growing evidence suggests that metabolism directly supports oncogenic signaling to foster tumor malignancy.[10,11] Thus, targeting cancer cell metabolic alterations may preferentially affect malignant cells and likely have broad therapeutic implications.

Voltage-dependent anion channel 1 (VDAC1) is a mitochondrial protein controlling cell energy and metabolic homeostasis and apoptosis.[12,13] VDAC1 mediates metabolic cross-talk between mitochondria and the cytosol, transporting metabolites, ions, nucleotides, Ca^{2+}, and more, thereby regulating mitochondrial activity. VDAC1 also plays a key role in apoptosis, participating in the release of apoptotic factors from mitochondria and interacting with anti-apoptotic regulators.[12,13] VDAC1 is highly expressed in different tumors,[13,14] including astrocytic tumors,[15] pointing to its significance in high energy-demanding cancer cells. We have demonstrated that abrogation of VDAC1 expression by 2′-O-Me-modified short interfering (si)RNA specific to human (h)VDAC1 (si-hVDAC1) reduced cellular ATP levels and cell growth and inhibited solid tumor development and growth in cervical and lung cancers.[14,16,17] As a key regulator of metabolic and energy reprogramming, disrupting cancer energy and metabolism homeostasis by targeting VDAC1 offers a potential anticancer therapy strategy.[18]

Here, we identified VDAC1 as a convergence point for GBM cancer cell metabolism, as siRNA-mediated VDAC1 depletion led to inhibition of tumor development by reversing reprogrammed metabolism, eliminating angiogenesis and stemness, and promoting cancer cell differentiation. These findings point to VDAC1 as an emerging cancer drug target.

Materials and Methods

See the Supplementary material for detailed Materials and Methods.

Cell Culture and Proliferation Assay

The GBM cell lines U-87MG, U-251MG, U-118MG, LN-18, C6, and GL-261; the human GBM patient-derived cells MZ-18 and MZ-327; the glioma-derived stem cell line G7; noncancerous HaCat cells; and primary human umbilical vein endothelial cells (HUVECs) and mouse primary brain cells (PBCs) were maintained at 37°C and 5% CO_2 in the recommended culture medium and supplements. Cells were transfected with non-targeting siRNA (si-NT) or si-VDAC1 using JetPRIME and analyzed for VDAC1 expression levels and cell growth (Supplementary material).

Mitochondrial Membrane Potential ($\Delta\Psi$) and Cellular ATP Levels

$\Delta\Psi$ and cellular ATP levels were assessed as described in the Supplementary material.

Xenograft Experiments

U-87MG and U-118MG cells were inoculated subcutaneously (s.c.) into the hind leg flanks of 8-week-old male nude mice. When tumor volume reached 50–80 mm^3, the mice were randomized into 2 groups and treated with si-NT or si-hVDAC1 mixed with in vivo JetPEI reagent, which was injected into the established s.c. tumors (50 nM final) every 3 days. At the end of the experiments, the mice were sacrificed and tumors were excised and processed for immunohistochemistry (IHC) or frozen in liquid nitrogen for immunoblotting and RNA isolation.

For the intracranial-orthotopic mouse model, U-87MG or MZ-18 cells were engrafted into a nude mouse brain using a stereotactic device. Mice were subjected to MRI (Supplementary material) and sacrificed, and their brains were excised and processed for IHC.

Experimental protocols were approved by the Institutional Animal Care and Use Committee.

RNA Preparation, qRT-PCR, DNA Microarray, and Gene Expression Pattern and Transcription Factor Profiling Array Analyses

Total RNA was isolated from si-NT or si-hVDAC1 treated tumors (TTs) and the generated cDNA was subjected to

Affymetrix microarray analysis or quantitative real-time (qRT)-PCR as described in the Supplementary material.

Immunohistochemistry, Immunofluorescence, and Immunoblotting

Formalin-fixed, paraffin-embedded sections of si-NT- or si-hVDAC1-TTs were stained with hematoxylin and eosin (H&E), probed with appropriate antibodies by IHC or immunofluorescent staining or by immunoblotting of tissue extracts and tissue (Supplementary material).

PLGA Encapsulation of siRNA

si-NT– and si-hVDAC1-loaded polyethylenimine-poly(lactic-co-glycolic acid) (PEI-PLGA) complexes were prepared by the solvent displacement method, as previously reported[19] and as detailed in the Supplementary material.

TUNEL Assay

Fixed tumor sections were processed for the terminal deoxynucleotidyl transferase deoxyuridine triphosphate nick end labeling (TUNEL) assay using the DeadEnd Fluorometric TUNEL system (Promega) according to the manufacturer's instructions (see Supplementary material).

Statistics and Data Analysis

Statistical significance is reported at $P < .05$(*), $P < .01$(**), or $P < .001$(***). For survival analysis, Kaplan–Meier plots were used.

Results

As VDAC1 is overexpressed in GBM (Fig. 1A), we explored the effects of VDAC1 depletion on GBM cancer hallmarks in vivo.

VDAC1 Depletion Inhibits Cancer Cell Growth and Tumor Development

Silencing VDAC1 expression by si-hVDAC1 in U-87MG and U-251MG cells led to marked decreases in VDAC1 levels (Fig. 1B–D) and in cell growth (Fig. 1E). These effects required only nanomolar concentrations and persisted several days posttransfection (Fig. 1B–E). si-NT had no significant effect on VDAC1 levels or cell growth (Fig. 1B–E). Similar results were obtained with other GBM cell lines, U-118MG, U-251MG, and LN-18 cells (Supplementary Fig. 1A–C). In noncancerous cells, HaCat, si-VDAC1 decreased VDAC1 expression, yet only slightly inhibited cell growth (Supplementary Fig. 1C). Similarly, siRNA recognizing both murine and human VDAC1 (si-VDAC1 m/h) was tested on mouse primary brain cells (PBCs) and was found less sensitive than on GBM cell lines (Fig. 1F, G)

The human siRNA sequence used (nucleotides 238–256) differed from the corresponding murine VDAC1 sequence by 4 nucleotides, and thus inhibited VDAC1 expression in U-87MG and U-251MG human cells but not in GL-261 murine cells (Supplementary Fig. 1A). In addition, 4 other si-VDAC1 sequences were tested and found to reduce both VDAC1 levels and cell growth (Supplementary Fig. 1F–I). Short interfering hVDAC1 specificity was further proved by restoring its inhibition of human U-87MG and U-251MG cell growth upon expressing mVDAC1 (Fig. 1H).

Cells expressing low VDAC1 levels possessed low mitochondrial membrane potential ($\Delta\Psi$) and cellular ATP levels (Fig. 1I, J).

The effect of si-hVDAC1 on U-87MG s.c. tumor xenografts established in nude mice was tested. Following tumor formation, mice were split into 2 matched groups, injected every 3 days with si-NT or si-hVDAC1, and tumor growth was followed. In si-NT–injected tumors, tumor volume increased by ~20-fold, whereas in si-hVDAC1-TTs, growth was markedly inhibited (Fig. 2A, B). Furthermore, when si-hVDAC1 was replaced by si-NT for 2 weeks, tumors grew at a similar rate as those continuously treated with si-hVDAC1 (Fig. 2B). Also, mouse weight decreased in si-NT- but not in si-hVDAC1-TTs (Supplementary Fig. 2A). All mice were sacrificed 36 days after the onset of treatment, tumors were excised, weighed (Supplementary Fig. 2B–C), and fixed and sections were IHC stained for VDAC1. si-NT-TTs were strongly immunostained, while as expected, si-hVDAC1-TT staining was very weak (Fig. 2C). These findings were confirmed by immunoblotting (Fig. 2D), which showed decreases in VDAC1 levels (70%–80%). Similar results were obtained with U-118MG cells in s.c. tumor xenografts (Supplementary Fig. 2D–G). Finally, TUNEL staining indicated that no significant apoptosis was induced in si-hVDAC1-TTs (Supplementary Fig. 2H).

To better mimic the clinical situation of GBM, we used intracranial-orthotopic xenografts[20] to examine si-hVDAC1 effectiveness in inhibiting tumor growth (Fig. 2E, F). si-NT– or si-hVDAC1–treated U-87MG cells were engrafted into nude mice brains and 22 and 33 days later, tumor growth was monitored by MRI. While tumors had developed in the si-NT–treated cells, no visible tumor was observed in the si-hVDAC1–treated cells (Fig. 2E, F).

To cross the blood–brain barrier (BBB) and deliver si-hVDAC1 to the brain, si-NT and si-hVDAC1 were encapsulated in nanoparticles made of PLGA/polyethylenimine/polyvinyl alcohol, shown to reach the brain and allow cargo release.[19] MRI imaging 20 (Fig. 2G, H) and 30 days (Supplementary Fig. 3A) post cell engraftment revealed 50% and 63% decreases in tumor volume, respectively, following i.v. treatment with PLGA-PEI–encapsulated si-hVDAC1 (400 nM). Mouse survival was also extended by about 2 weeks upon si-hVDAC1–PLGA treatment (Fig. 2I). These results suggest that PLGA-PEI–encapsulated si-hVDAC1 is delivered to the brain.

Finally, using the human GBM patient-derived MZ-18 cells in intracranial-orthotopic xenografts (PDX) and i.v.-injected PLGA-PEI–encapsulated si-NT or si-hVDAC1, we

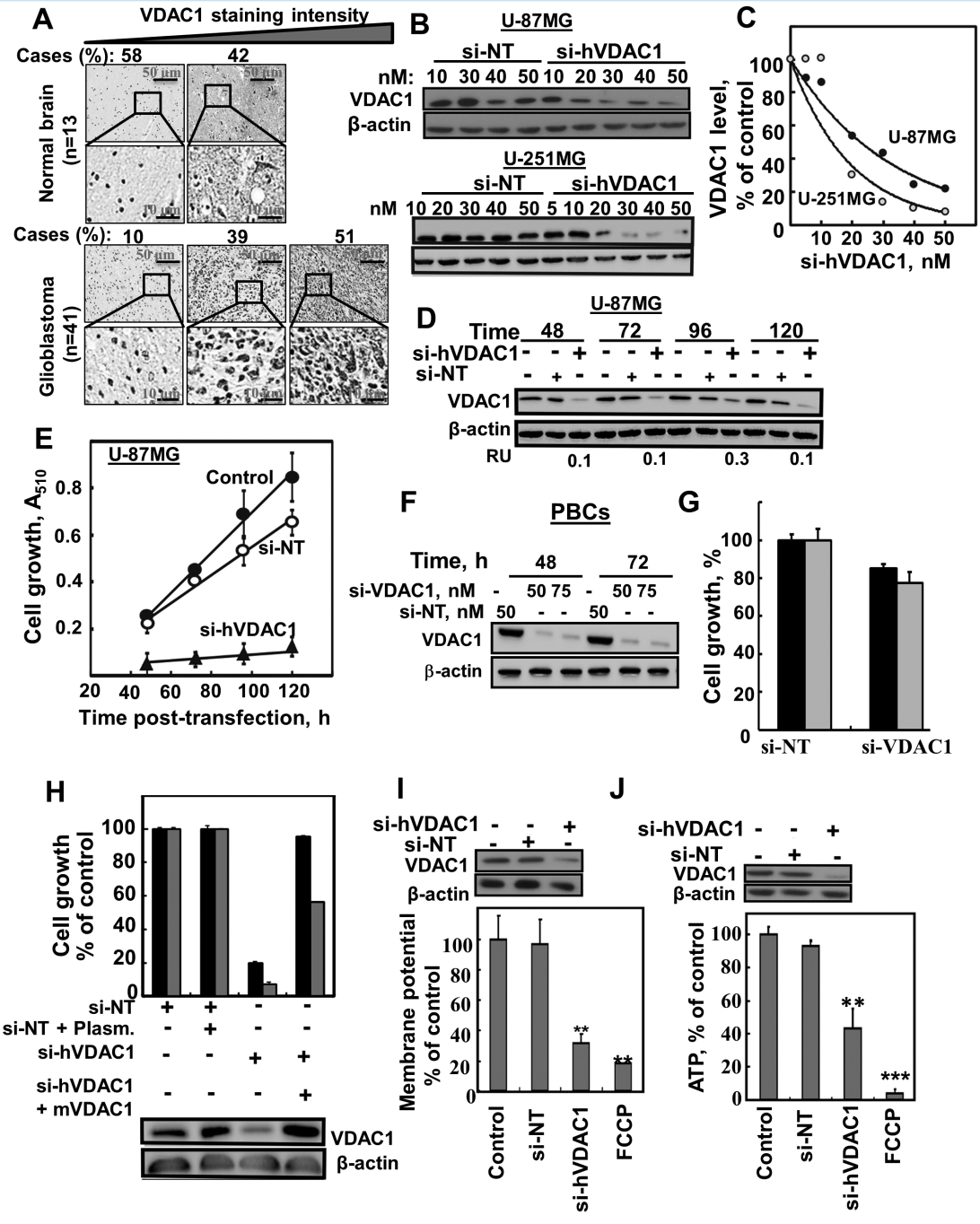

Fig. 1 si-hVADC1 inhibited cell growth and reduced energy production in GBM cell lines. (A) IHC staining of VDAC1 of human normal brain (n = 13) or GBM (n = 41) in tissue microarray slides (Biomax). Percentages of sections stained at the intensity indicated are shown. (B, C) U-87MG and U-251MG cells were treated for 48 h with si-NT or si-hVDAC1 and analyzed for VDAC1 levels by immunoblotting. (D, E) U-87MG cells were treated with si-NT or si-hVDAC1 (50 nM) and at the indicated time were analyzed for VDAC1 levels (D) or for cell growth using a sulforhodamine B assay (E). (F, G) Mouse primary brain cells (PBCs) were incubated (48 and 72h) with si-NT or si-VDAC1(M/H) and analysed for VDAC1 levels (F) and cell growth (G) (n = 3). (H) U-87MG (black bars) and U-251MG (gray bars) cells were treated with si-NT or si-hVDAC1, transfected 24 h later with pcDNA4/TO, either empty or encoding mVDAC1, and 2 h later, cell growth was analyzed (n = 3). $\Delta\Psi$ (I) and ATP (J) levels were analyzed in U-87MG cells (n = 3). FCCP (carbonyl cyanide-4-(trifluoromethoxy)phenylhydrazone), $^{**}P \leq .01$; $^{***}P \leq .001$ (25 μM) served as control for decreasing $\Delta\Psi$ and ATP levels. RU = relative unit.

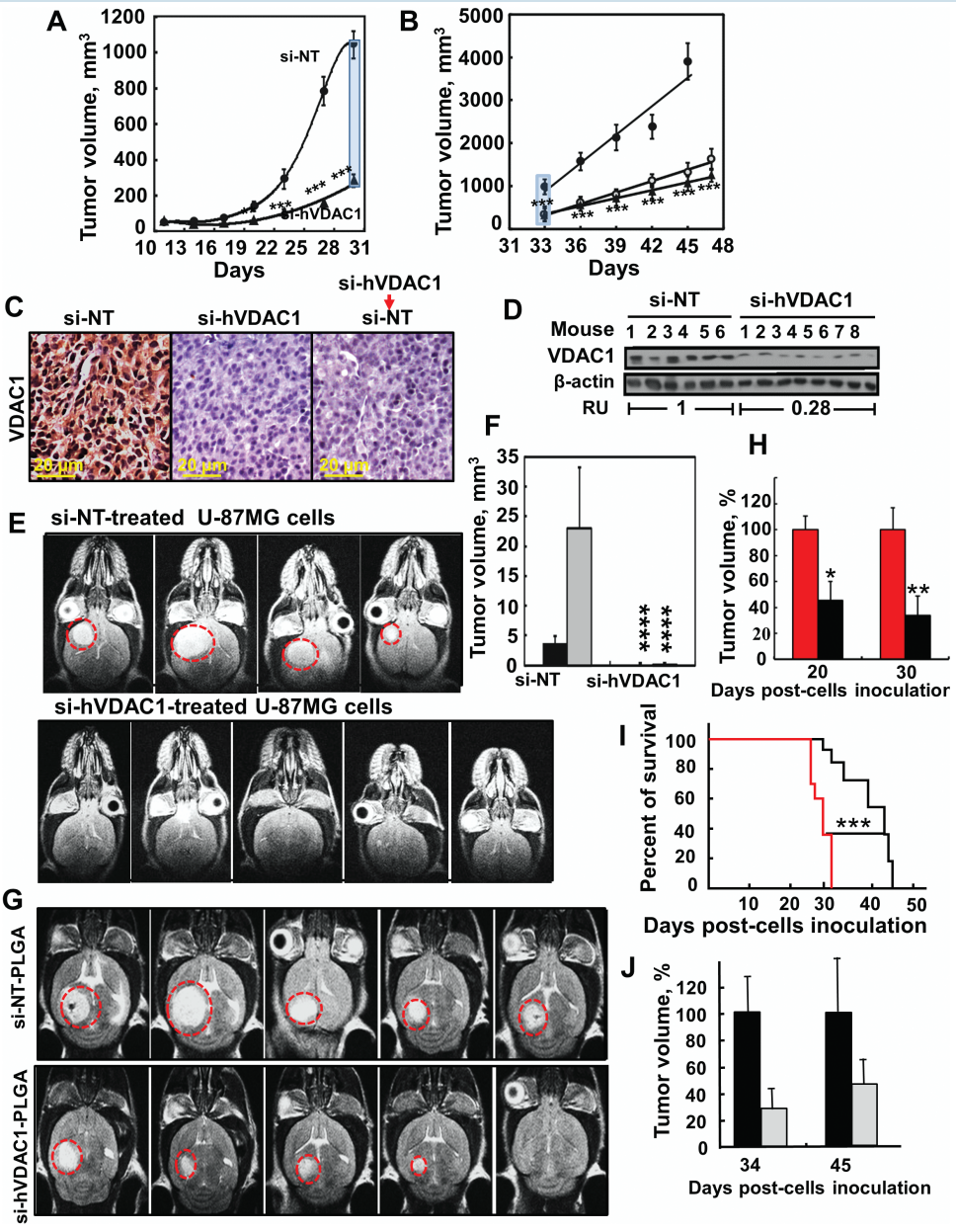

Fig. 2 si-hVADC1 inhibition of tumor growth in vivo. (A) U-87MG cells were s.c. inoculated into nude mice. On day 13, the mice were divided into 2 groups and xenografts were injected every 3 days with si-NT (●, 8 mice) or si-hVDAC1 (▲, 16 mice) to a final concentration of 50–60nM (***$P \leq$ .0001). (B) On day 33, the si-hVDAC-treated mice were subdivided into 2 groups (8 mice each). One group (▲) continued si-hVDAC1 treatment, the other switched to si-NT (○) treatment. si-NT-TTs and si-hVDAC1-TTs sections stained for VDAC1 by IHC (C) or immunoblot (D). RU = average relative units. (E) Orthotopic GBM, MRI of brains 33 days post-engraftment with U-87MG cells treated with si-NT or si-VDAC1. (F) Calculated tumor volume after 22 (black bars) and 33 days (gray bars). Results = mean ± SEM (n = 4–5), ****$P \leq$ .0001. (G) MRI of brains engrafted with U-87MG cells, 22 days after cell engraftment and treatment start. Two days post-engraftment, the mice were divided into 2 groups (6 mice each) and injected i.v. every 3 days with 100 μL of si-NT- or si-hVDAC-encapsulated-PLGA nanoparticles (400 nM siRNA). (H) Calculated tumor volume after 20 and 30 days. Red and black bars representing tumor volume of mice treated with si-NT- or si-hVDAC-encapsulated PLGA nanoparticles, respectively. Results = mean ± SEM (n = 6), *$P \leq$ .05; **$P \leq$ .01. (I) Mice survival over time of si-NT-PLGA- (red line) and si-hVDAC1-PLGA nanoparticle (black line) treated mice is presented in the cumulative Kaplan–Meier survival curves. ***$P \leq$ .001. (J) Orthotopic MZ-18 cells (10×10^4) (PDX) were engrafted into mice brains and 2 days later, the mice were divided into 2 groups (6 mice each) and injected i.v. every 3 days with si-NT- (black bars) or si-hVDAC (gray bars)-encapsulated PLGA-PEI nanoparticles (400 nM siRNA). Tumor volume was calculated from MRI taken 34 days post cell engraftment, and then 10 days after treatment termination (day 45).

showed that 34 days post cell engraftment, si-hVDAC1 treatment decreased tumor volume by 70% (Fig. 2J), as analyzed by MRI (Supplementary Fig. 3B). Ten days after termination of treatment, tumor volume was analyzed and the decrease was 50%.

Taken together, these results show VDAC1 depletion leading to inhibition of cell proliferation and tumor growth in both subcutaneous and intracranial mouse models.

VDAC1 Depletion Reverses Reprogrammed Cancer Cell Metabolism and Inhibits Cell Proliferation

The metabolic alterations that occur during malignant transformation contribute to elevated glycolysis.[6] si-hVADC1-TTs showed high decreases in glucose transporters (Glut1), hexokinase type I (HK-I), glyceraldehyde dehydrogenase (GAPDH), and lactate dehydrogenase (LDH) levels compared with si-NT-TTs (Fig. 3A, B, D, E). Expression levels of the Krebs cycle enzyme, citrate synthase, mitochondrial electron transport complex IVc, and ATP synthase 5a were also highly reduced in si-hVDAC1-TTs (Fig. 3C, E), consistent with alterations in oxidative phosphorylation (OXPHOS). Similar results were obtained by qRT-PCR (Fig. 3F) and with U-118MG xenografts (Supplementary Fig. 4). In the orthotopic model, tumors derived from si-NT–treated mice expressed high levels of Glut1 and VDAC1 (Fig. 3G). Together, these findings point to a reversal of the metabolic reprogramming of cancer cells upon VDAC1 depletion.

As si-hVDAC1 tumor treatment reduces metabolism, inhibition of cell proliferation was expected. Indeed, si-hVDAC1-TTs markedly decreased (>80%) the expression level of the cell proliferation factor Ki-67, as shown by IHC staining or qRT-PCR (Fig. 3H–J). A similar decrease in the mRNA level of the proliferating cell nuclear antigen (PCNA) was also observed (Fig. 3J).

Finally, the level of epidermal growth factor receptor (EGFR), associated with increased proliferation and migration of GBM cells, was decreased in si-hVDAC1-TTs, as revealed by IHC and immunoblotting (Fig. 3K, L).

VDAC1 Depletion Induces Expression of Differentiation-Associated Proteins

Since altering cancer metabolism is proposed to affect cell differentiation,[21] we analyzed the levels of several differentiation markers in si-NT-TTs and si-hVDAC1-TTs. Sections of normal and GBM-affected human brain were H&E stained. Normal brain showed astrocytes, a few small vessels, and mainly fibrillary stroma (Fig. 4A). In contrast, GBM sections showed large irregular cells with atypical nuclei (Fig. 4B). Staining of normal brain sections for glial fibrillary acidic protein (GFAP), expressed by astrocytes, showed cells with long and marked processes (Fig. 4A). GFAP staining of GBM sections showed cells with no processes (Fig. 4B).

H&E-stained si-NT-TT sections revealed cells with large nuclei (Fig. 4D), as in GBM patients (Fig. 4B). In contrast, si-hVDAC1-TTs showed astrocyte-like cell morphology with long and marked processes (Fig. 4C).

Next, immunostaining for mature neuronal markers, such as microtubule-associated protein 2 (MAP2) and tubulin beta 3 (TUBB3) (Fig. 4E, F; Supplementary Fig. 5), showed that both were highly expressed in si-hVDAC1-TTs, as also demonstrated by qRT-PCR (Fig. 4G). These results indicate that si-hVDAC1 treatment induced morphological changes in tumor cells to resemble normal brain cells and altered expression of neuronal markers, suggesting differentiation of tumor cells into astrocyte- and neuron-like cells.

To verify possible cell differentiation stages of si-hVDAC1-TTs, markers of cell differentiation stages were screened using qRT-PCR. Reductions (4-120-fold) were found in the levels of markers for early and late neuronal precursor cells, of immature astrocytes and neurons, and of the neuronal precursor and progenitor marker nestin, brain lipid-binding protein (BLBP), stage-specific embryonic antigen 1 (SSEA1/CD15), tenascin C, and aldehyde dehydrogenase 1L1 (ALDH1L1). At the same time, increases (15-120-fold) were found in the levels of markers associated with mature astrocytes and neurons (GFAP, TUBB3, and MAP2) (Fig. 4G).

These findings were further supported by immunofluorescent staining of tumor sections. Nestin staining was highly decreased, while TUBB3, GFAP, and glutamate decarboxylase 1 (GAD1/GAD67), involved in gamma-aminobutyric acid synthesis, were strongly stained (Fig. 4H). Similar results were obtained with U-118MG tumors (Supplementary Fig. 5). These results indicate that si-hVDAC1 tumor treatment led GBM-induced precursor cells to differentiate toward mature astrocyte- and neuron-like cells.

VDAC1 Depletion Alters Transcription Factor Expression Profiles

To better understand the molecular mechanism underlying the cell signaling altered by si-hVDAC1-TT leading to cell differentiation, we screened for changes in the expression levels of transcription factors (TFs) in the nuclear fraction using a cancer stem cell TF activation profiling plate array (Fig. 5A). si-hVDAC1-TTs expressed increased levels of tumor suppressor TFs, such as p53, forkhead box (FOXO3), PR-domain-containing 14 (PRDM14), and signal transducer and activator of transcription 3 (STAT3).

Expression levels of the major TFs p53, hypoxia-inducible factor 1 alpha (HIF-1α), and c-Myc, known to regulate metabolism, cell growth, proliferation, and differentiation,[22] were significantly affected by si-hVDAC1 treatment. Levels of p53 were elevated in si-hVDAC1-TTs, while the expression levels of HIF-1α and c-Myc were reduced, as revealed by TF activation profiling assay, qRT-PCR, and immunoblotting (Fig. 5A–C). The level of activator protein (AP2), involved in tumorigenesis and possibly acting as a tumor suppressor, was decreased in si-hVDAC-TTs (Fig. 5A).

These results (Figs. 4, 5) thus present a complex set of effects of VDAC1 depletion on a network of key regulators of cell metabolism, leading to cancer cell differentiation to mature neuronal-like cells.

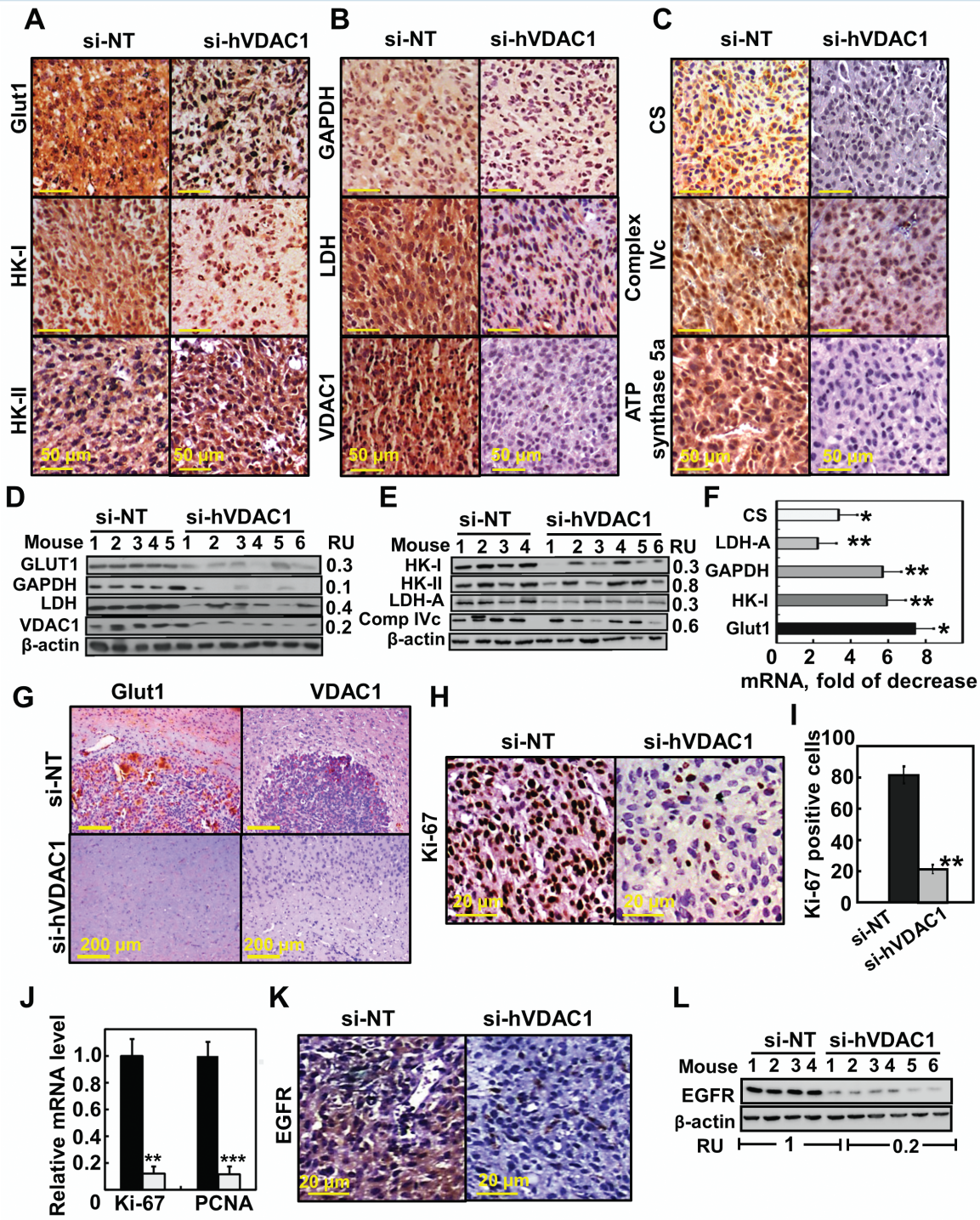

Fig. 3 Reversal of the U-87MG tumor cell reprogrammed metabolism by si-hVDAC1 treatment. (A–C) IHC of s.c. si-NT-TTs or si-hVDAC1-TTs stained for the indicated antibodies. (D, E) Immunoblot of selected proteins. RU = relative unit. (F) Levels of mRNA of metabolic enzymes in si-hVDAC1-TTs relative to those in si-NT-TTs. Results = mean ± SEM (n = 3–5), *$P \leq .05$; **$P \leq .01$. (G) Representative IHC sections from brains engrafted with si-NT- or si-hVDAC1–treated U-87MG cells, 22 days after cell grafting, stained for Glut1 and VDAC1. (H, I) IHC of s.c. si-NT-TTs and si-hVDAC1-TTs stained for Ki-67; positive cells were counted over several fields. (J) Analysis by qRT-PCR of Ki-67 and proliferating cell nuclear antigen (PCNA) mRNA levels in si-NT- (black bars) and si-hVDAC1 (gray bars)-TTs. Results = mean ± SEM (n = 3–5), **$P \leq .01$; ***$P \leq .001$). (K, L) IHC and immunoblot analyses of epidermal growth factor receptor.

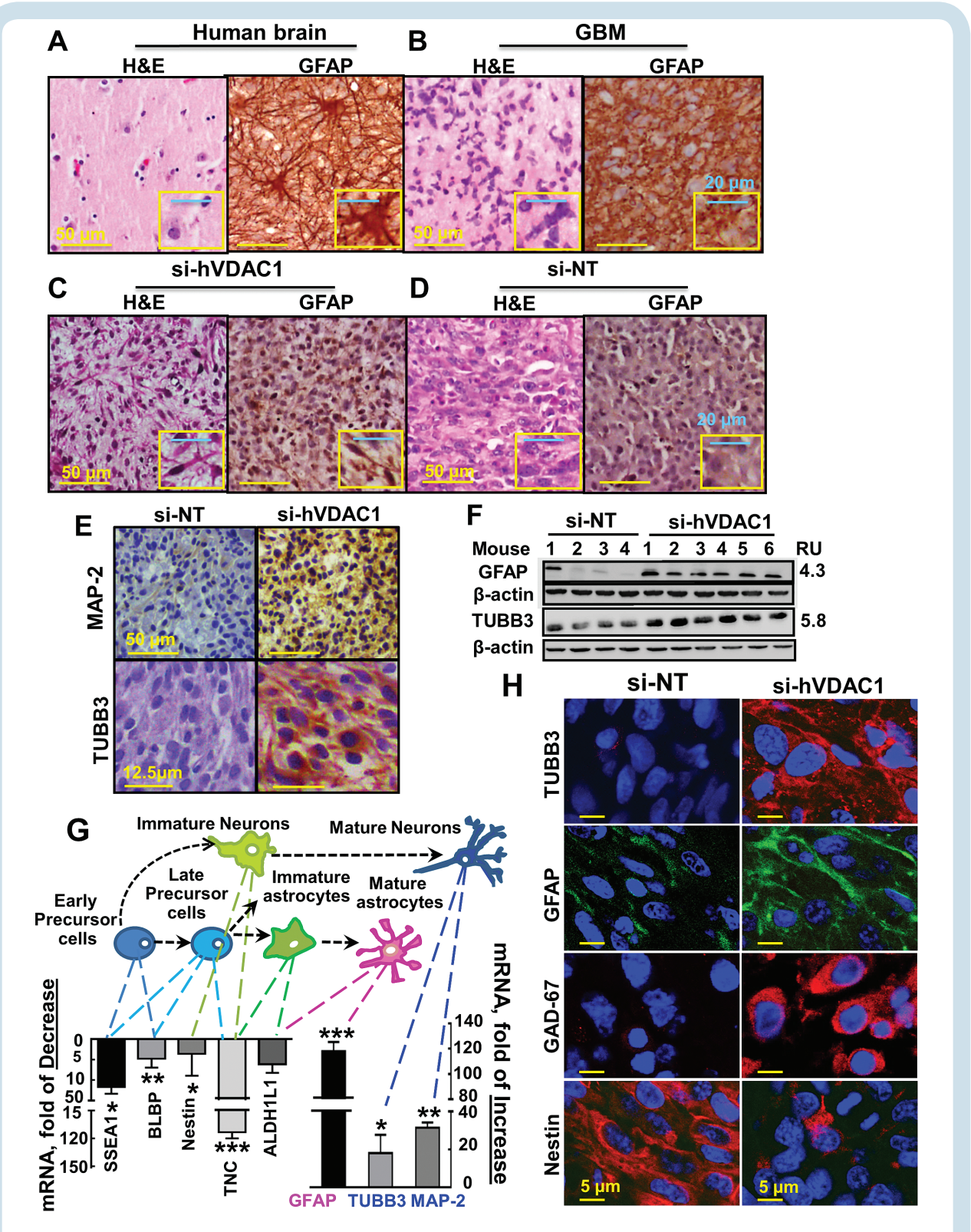

Fig. 4 U-87MG cells in si-hVDAC1-TTs: morphological changes and expression of neuronal markers. Human normal (A), GBM brains (B), or hVDAC1-TTs (C) or si-NT-TTs (s.c.) (D) stained with H&E or anti-GFAP antibodies. (E) si-hVDAC1-TTs or si-NT-TTs sections stained with anti–Map-2 or anti-TUBB3 antibodies. (F) Immunoblot of GFAP and TUBB3 in si-NT-TTs and si-hVDAC1-TTs. RU = relative units. (G) Schematic presentation of early precursor cell differentiation into mature astrocytes via several possible intermediate states: late precursor cells, immature astrocytes, or neurons via immature neurons. Levels of mRNA markers specific for each state in s.c. si-hVDAC1-TTs relative to those in si-NT-TTs are presented. Results are the mean ± SEM (n = 3–5); *$P \leq .05$; **$P \leq .01$; ***$P \leq .001$. (H) Immunofluorescent staining of si-NT-TT– and si-hVDAC1-TT–derived sections for nestin, GFAP, TUBB3, and GAD67.

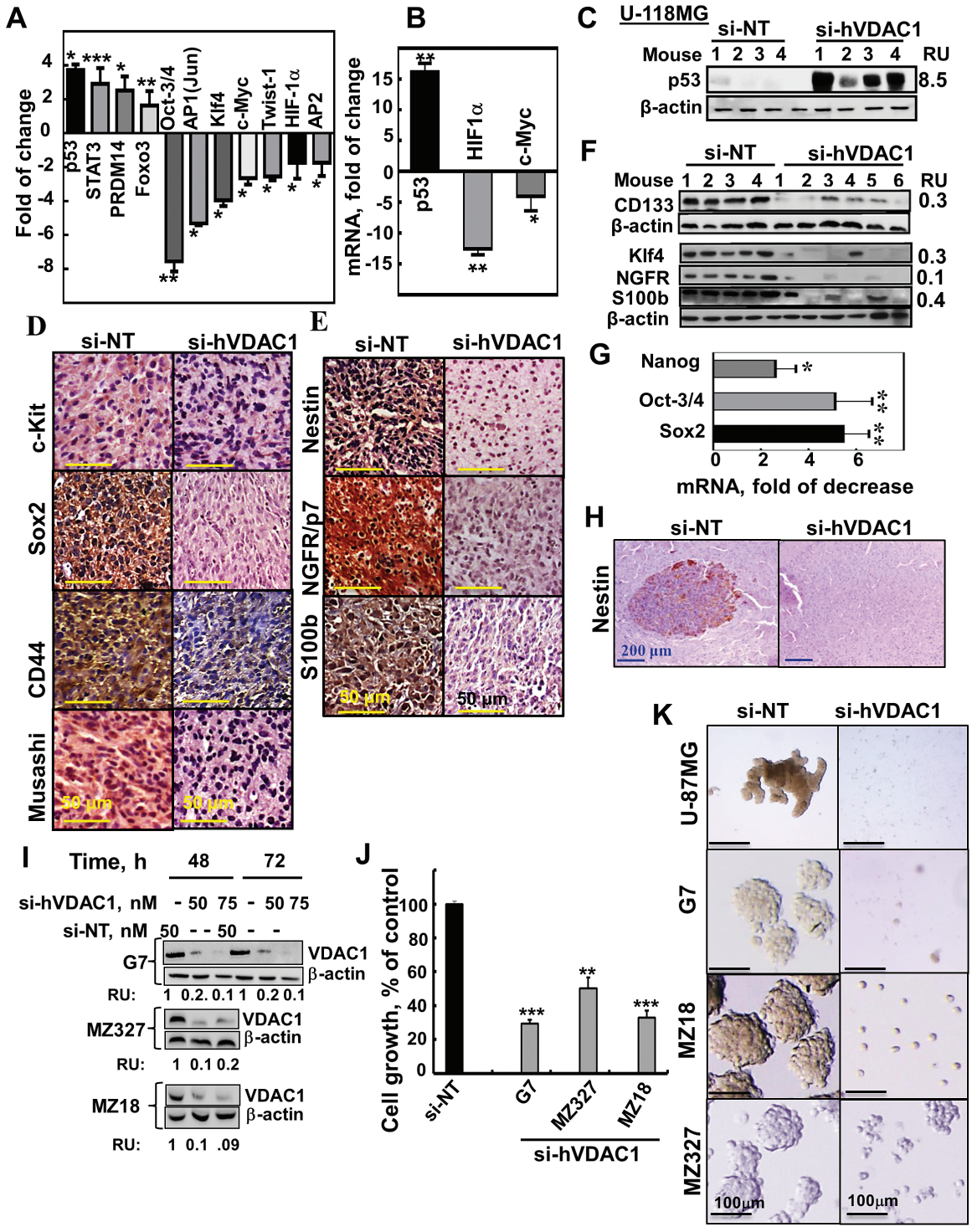

Fig. 5 TF levels and stem cell marker expression are altered in si-hVDAC1-TTs and inhibition of cancer neurosphere formation. (A) Stem cell TF activation profiling was analyzed in s.c. U-87MG si-NT- or si-hVDAC1-TTs. (B) Analysis by qRT-PCR of p53, c-Myc, and HIF-1α mRNA levels in si-hVDAC1-TTs, relative to si-NT-TTs. Results = mean ± SEM (n=3–5); $^{*}P \leq .05$; $^{**}P \leq .01$. (C) Immunoblot of p53 in si-NT-TTs and si-hVDAC1-TTs derived from U-118MG cells. (D, E) IHC and immunoblot (F) staining for stem cell markers and qRT-PCR analysis of Sox2, Oct3/4, and Nanog (G) of si-NT- or si-hVDAC1-TTs sections. Results = mean ± SEM (n = 3–5), $^{*}P \leq .05$; $^{**}P \leq .01$. (H) Nestin-stained sections from brains 22 days post-grafting treated with si-NT– or si-hVDAC1–treated U-87MG cells. (I–K) G7, MZ-18, and MZ327 cells were treated with si-NT or si-hVDAC1 and after 48 and 72 h, the cells were analyzed for VDAC1 levels (I) or cell growth using a sulforhodamine B assay (J). Results are the mean ± SEM (n = 3); $^{**}P \leq .01$; $^{***}P \leq .001$. (K) Neurosphere formation in si-NT– or si-hVDAC1–treated U-87, G7, MZ-18 and MZ-327 cells in stem cell–specific medium.

Tumor Treatment with si-hVDAC1 Eliminates Cancer Stem Cell Markers and Inhibits Neurosphere Formation

The decrease in the levels of TFs associated with stemness in si-hVDAC1-TTs (octamer-binding transcription factor 3 or 4 [Oct3/4], AP1(Jun), Twist, and Kruppel-like factor 4 (Klf4) [Fig. 5A]) and with invasion[2] (Supplementary Fig. 7A, B) led us to further analyze the effects of VDAC1 depletion on the expression of GSC-associated markers. si-hVDAC1 treatment markedly decreased the expression of GSC markers, such as CD133, sex determining region Y–box 2 (Sox2), Klf4, Musashi, nestin, nerve growth factor receptor (NGFR), S100b, and CD44, as evaluated by IHC and immunoblotting (Fig. 5D–F) and by qRT-PCR (Fig. 5G), which revealed decreases of several-fold in Sox2, Oct3/4, and Nanog mRNA levels. Similar results were obtained with U-118MG xenografts (Supplementary Fig. 6A, B). The orthotopic tumors derived from si-NT–treated mice showed high levels of nestin (Fig. 5H). Thus, si-VDAC1 tumor treatment resulted in a strong decrease in GSC markers by arresting cell proliferation (Fig. 3H) and/or promoting differentiation (Fig. 4).

The effect of si-hVDAC1 treatment on stem cells was also demonstrated by analyzing neurosphere formation using neuro-stem cell medium. U-87MG, the glioma-derived G7 stem cell line, and the human GBM patient-derived cells, MZ-18 and MZ-327, were treated with si-NT or si-hVDAC1, showed decreased VDAC1 levels, and inhibited cell growth (Fig. 5I, J). Neurospheres were formed in the si-NT–treated but to a lesser extent in si-hVDAC1–treated cells (Fig. 5K). The reduced potential of neurosphere formation by reducing VDAC1 levels suggests a decrease in GSC levels upon metabolic reprogramming.

VDAC1 Depletion and Tumor Microenvironment

The tumor invasion and metastatic potential is enhanced by the epithelial-mesenchymal transition (EMT).[23] To follow EMT, we analyzed si-NT- and si-hVDAC1-TTs for the expression of EMT cell markers (Supplementary Fig. 6C–E). Immunostaining of si-hVDAC1-TTs showed a decrease in the mesenchymal cell markers N-cadherin and vimentin and an increase in E-cadherin, an epithelial cell marker,[23] compared with their levels in si-NT-TTs (Supplementary Fig. 6C, D). Similar results were obtained with qRT-PCR, showing the mesenchymal markers Twist, Zeb1, Zeb2, Snail1, Snail2, and N-cadherin[24] to be decreased 3-12-fold in si-VDAC1-TTs (Supplementary Fig. 6E). These results show that EMT was reversed in si-hVDAC1-TTs leading to attenuated invasive potential of GBM cells (Supplementary Fig. 7A, B).

A solid tumor requires blood supply to continue growing and thus promotes angiogenesis, with GBM being highly angiogenic and invasive.[1] Immunostaining of endothelial cells from si-hVDAC1-TT for CD31 showed a major decrease in the number of blood vessels, with microvessel density quantitation revealing about 80% decrease (Supplementary Fig. 7C, D).

In GBM, as in many other cancers, high levels of vascular endothelial growth factor (VEGF) are expressed in tumors to stimulate angiogenesis. VEGF/A levels were highly decreased in si-hVDAC1-TTs (Supplementary Fig. 7E, F). IHC analysis of si-hVDAC1-TTs also showed decreased levels of the tumor-associated macrophage (TAMs) marker F4/80 (Supplementary Fig. 7G). Similarly, DNA microarray analysis (Supplementary Table 4) also showed that si-hVDAC1 treatment affected the expression of angiogenesis-, EMT-, and invasion-related genes, reducing VEGF/A, transforming growth factor β (TGF-β), HIF-1α, metalloproteinases, and extracellular matrix and cell adhesion components while increasing angiogenic and matrix metalloproteinase inhibitors.

The VDAC1 Inhibitor Itraconazole Directly Interacts with Purified VDAC1 to Inhibit Cell and Tumor Growth

Recently, VDAC1 was identified as a target of itraconazole in endothelial cells.[25] Therefore, its interaction with purified VDAC1 and effects on GBM-derived cells were studied.

Itraconazole reduced channel conductance of planar lipid bilayer-reconstituted VDAC1 at all voltages tested (Supplementary Fig. 9A, B). Next, we tested for a direct interaction of itraconazole with VDAC1 using microscale thermophoresis (Supplementary Fig. 9C), noting a dissociation constant of 120 μM. These results are the first demonstration of direct interaction of itraconazole with VDAC1.

Itraconazole similarly inhibited growth of HUVEC, U-87MG, U-251MG, U-118MG, and L-18 cells, while mouse PBCs were less sensitive (Supplementary Fig. 9D).

The effect of itraconazole on U-87MG s.c. tumor xenografts was tested (Supplementary Fig. 9E, F). Itraconazole decreased tumor volume 35% and 64% when treated for 10 days with 30 μM and 100 μM, respectively. The high itraconazole concentrations required for tumor growth inhibition are in agreement with the binding affinity to VDAC1 and the high itraconazole concentration (75 mg/kg), given orally, to decrease tumor volume by ~59% after 20 treatment days.[26]

Finally, in GBM patient-derived MZ-18 cells in the intracranial PDX model, it was shown that when given in drinking water (but not when administered i.v.), itraconazole greatly decreased tumor growth (Supplementary Fig. 9G).

The Gene Expression Profile of si-hVDAC1-TTs Is Highly Modified

To explore changes in the patterns of gene expression in si-hVDAC1-TTs versus si-NT-TTs, we performed Affymetrix DNA microarray analysis (Fig. 6A, B). Such analysis revealed 4493 significantly changed genes (≥2-fold change, false discovery rate <0.05), which were clustered to 1998 downregulated genes (cluster 1) and 2495 upregulated genes (cluster 2) in the si-hVDAC1-TTs (Fig. 6A). Functional analysis (Gene Ontology system) revealed alterations in key functions and pathways related to tumorigenicity (Fig. 6B).

The downregulated group (Fig. 6B) was highly enriched for genes related to cell cycle and DNA repair and to the mitochondrion, such as genes encoding Krebs cycle and OXPHOS enzymes, in agreement with IHC and immunoblotting results (Fig. 3). The upregulated group (Fig. 6B) was enriched for genes related to the regulation of transcription factors and the WNT pathway. Remarkably, 67 genes were associated with neuronal differentiation.

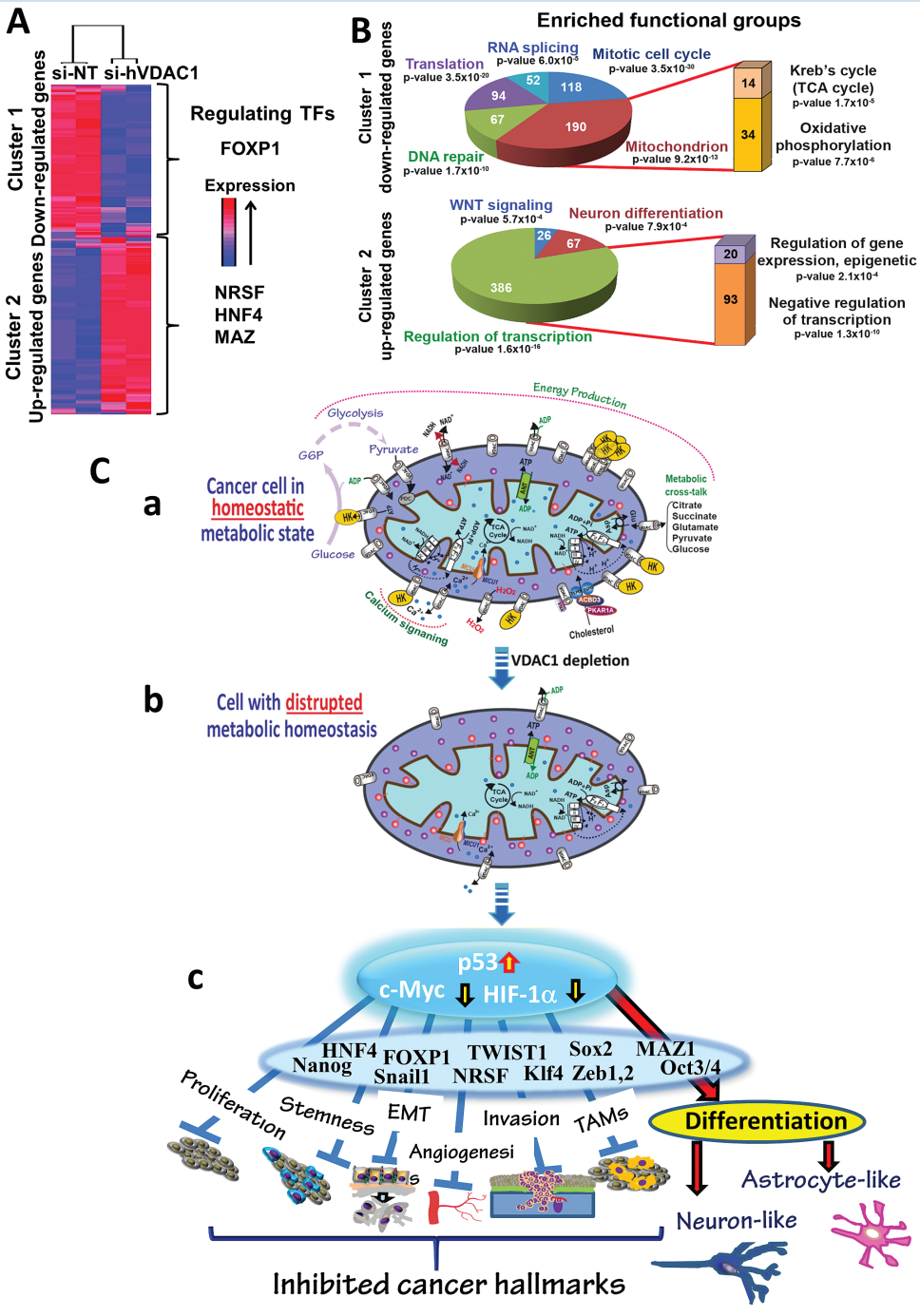

Fig. 6 VDAC1-depletion and metabolic reprogramming leading to alterations in key TF levels and biological processes: a reversal of oncogenic properties and cell differentiation. (A, B) DNA microarray and bioinformatics analyses of si-hVDAC1- and si-NT-TTs (s.c.) reveal alterations in key TF levels and biological processes. RNA isolated from U-87MG si-hVDAC1- and si-NT-TTs was subjected to Affymetrix DNA microarray analysis. (A) Clustering of the 4493 differentially expressed genes: blue to red colors indicate expression levels. Promoter analysis indicates binding sites enrichment for FOXP1 (367 genes, $P = 3.4 \times 10^{-20}$) in cluster 1, and NRSF (1310 genes, $P = 1.3 \times 10^{-84}$), HNF4 (1161 genes, $P = 5.8 \times 10^{-38}$), and MAZ (678 genes, $P = 1.2 \times 10^{-22}$) in cluster 2. (B) Functional analysis of clusters 1 and 2 based on the Gene Ontology system. The number of genes associated with the indicated function is presented. (C) A schematic presentation of mitochondria in cancer cell VDAC1 depletion and metabolic reprogramming leading to a reversal of oncogenic properties and cell differentiation. Before treatment with si-hVDAC1, cancer cells maintain homeostatic energy and metabolic states, with HK bound to VDAC1, accelerating glycolysis and mitochondrial function to allow sufficient ATP and metabolite precursor levels to support cell growth and survival (a). VDAC1 depletion leads to dramatic decreases in energy and metabolite generation (b). This leads to changes in master metabolism regulator (p53, HIF1-α, and c-Myc) expression levels, which alter the expression of TFs associated with the oncogenic properties of stemness, EMT, cell proliferation, invasion, TAMs, and angiogenesis, while leading to differentiation into astrocyte- or neuron-like cells (c).

Promoter analysis of the differentially expressed genes in si-hVDAC1-TTs revealed enrichment of several TF binding sites (BSs). The downregulated group showed high enrichment in genes encoding proteins with BSs for FOXP1. FOXP1 may act either as a transcriptional activator or repressor or as an oncogene or tumor suppressor.[27] Our analysis suggests that FOXP1 acts as a transcriptional activator and as an oncogene, as its level was downregulated (Supplementary Fig. 8). In the upregulated group, BSs for 3 main TFs were highly enriched (Fig. 6A). Neuron-restrictive silencer factor (NRSF), a transcriptional repressor of neuronal genes in nonneuronal cells,[28] was downregulated in si-hVDAC1-TTs (Supplementary Fig. 8B), allowing for differentiation into neuronal-like cells. The same was true for hepatocyte nuclear factor 4 (HNF4), a central regulator of hepatocyte differentiation, and myelocytomatosis-associated zinc finger protein (MAZ), which regulates c-Myc and HRAS.[29] Together, HNF4 and MAZ co-regulate neural stem cell differentiation.[30] Downregulation of HNF4 and MAZ in si-hVDAC1-TTs (Supplementary Fig. 8) is in agreement with the differentiation of GBM cells in these tumors (Fig. 4).

Discussion

GBM, as a highly heterogeneous tumor harboring multiple genetic alterations,[1] presents a daunting challenge in terms of treatment and thus requires new molecular-targeted and therapeutic approaches.[31] We demonstrate in subcutaneous and intracranial-orthotopic GBM models, and using both GBM cell lines and patient-derived cells, that VDAC1 depletion by si-hVDAC1 resulted in reprogrammed metabolism and an inhibition of stemness, angiogenesis, EMT, and invasiveness. Thus, the presented results explored metabolism, controlled by VDAC1, as an emerging GBM treatment target, controlling cancer cell reprogramming, and demonstrated the intricate interplay between metabolism and the oncogenic signaling network. We showed that VDAC1 depletion resulted in multifactorial responses with global changes in the expression of proteins involved in cancer cell metabolism, proliferation, angiogenesis, stemness, and differentiation into neuronal-like cells and in the TFs mediating these effects (Fig. 6C).

The central role of VDAC1 in cell energy and metabolism is reflected in its overexpression in many tumors, including glioma (Fig. 1A), and in VDAC1 depletion, impairing cancer cell energy and metabolic homeostasis.[13] Upregulated Glut1 and HK foster enhanced aerobic glycolysis and are common hallmarks of many cancers.[32] VDAC1 depletion resulted in inhibited cell growth, concomitant with marked decreases in Glut1, HK-I, GAPDH, and LDH and of Krebs cycle and OXPHOS enzymes (Fig. 3). This is in line with studies suggesting that cancer cells use both glycolysis and OXPHOS.[9,33]

As metabolism is a promising cancer target,[34] several drugs targeting cancer metabolism are being developed. Here, we present a new concept of modulating cancer cell metabolism by depleting VDAC1, leading to reversal of GBM cell energy and metabolic reprogramming, involving alterations in the expression profile of TFs and genes associated with metabolic regulation.

Our data showed that VDAC1 depletion prevented neurosphere formation and induced cancer stem cells to differentiate into mature astrocyte- and neuron-like cells. Recent studies have reinforced the hypothesis that human gliomas contain a neural stem cell lineage[35,36] capable of self-renewal and differentiation into multiple lineages.[3] Tumor treatment with si-hVDAC1 apparently eliminated GSCs, EMT, and invasion, as reflected in the high decrease in expression of factors known to control stemness, including CD133 associated with radio- and chemoresistant subpopulations of GBM cells.[36,37] The decrease in GSC levels could be due to proliferation inhibition and/or differentiation, as reflected in morphological changes and increased expression of the neuronal differentiation markers (Fig. 4; Supplementary Fig. 5).

VDAC1 depletion leading to cell differentiation is further supported by bioinformatics promoter analysis of genes differentially expressed in si-hVDAC1-TTs, pointing to enrichment for BSs of TFs involved in cell differentiation (Supplementary Figs. 7A, 8). FOXP1 was overexpressed in a cohort of GBM patients, with its silencing leading to tumor growth inhibition.[38] NRSF was also found to be enriched in GBM, with its knockdown strongly reducing tumor-initiating capacity in vivo.[39] Finally, HNF4 and MAZ were reported to co-regulate neural stem cell differentiation via Rho guanosine diphosphate [GDP]-dissociation inhibitor gamma (Rho-GDIγ).[30] These TFs were downregulated in si-hVDAC1-TTs, thus leading to cell differentiation.

Hence, resting on cell morphological changes, increased expression of mature neuronal and astrocytic markers, and the decreased expression of GSC markers (Figs. 4, 5), we suggest that upon VDAC1 depletion, GSCs in U-87MG and U-118MG cell–derived tumors are capable of in vivo differentiation toward mature neuron- and astrocyte-like cells that barely replicate, thereby possibly preventing tumor regrowth.

Finally, the connection between VDAC1 depletion and alterations in gene expression, including those encoding TFs, may be mediated via the proposed link between metabolism and epigenetics,[9,40] a link that has been explored in tumorigenesis.[41]

Cancer cell metabolism also modifies tumor microenvironment.[42] VDAC1 depletion resulted in strongly decreased angiogenesis and VEGF levels (Supplementary Fig. 7E, F). Anti-angiogenesis therapy with VEGF receptor inhibitors has been a focal area in cancer drug discovery for over a decade, including use as GBM therapy,[43] albeit with limited success or organ-specific toxicity. Hence, si-VDAC1 is a potential anti-angiogenesis agent.

EMT is associated with increased cell migration/invasivity and cancer progression.[23] si-hVDAC1 treatment changed the expression of proteins involved in EMT and extracellular matrix components and of TAMs, associated with tumor inflammation, suggesting attenuated tumorigenic processes.

Finally, one can ask: how does VDAC1 depletion reverse cancer cell oncogenic properties? Changes in cancer cell metabolism contribute to the oncogenic process.[5,6] A proposed model connecting rewired cancer cell energy and metabolism, as induced by VDAC1 depletion, and cell differentiation, as mediated via alteration in a panel of genes and TFs, is presented in Fig. 6C. Clearly, depletion of VDAC1 affects critical functional nodes in the oncogenic network.

As mitochondria are not only energy generators but also factories synthesizing indispensable molecules for cancer cellular biosynthesis, growth, and proliferation, it is not surprising that a lack of VDAC1 led to mitochondrial dysfunction and an arrest of cell growth. This is supported by the effect of itraconazole in inhibiting tumor growth (Supplementary Fig. 9E–G).

The reprogramming of tumor metabolism often involves genetic alterations that can be traced to a triad of the TFs c-Myc, HIF-1α, and p53, which orchestrate expression of a group of genes, including those supporting glycolytic metabolism.[22] In si-hVDAC1-TTs, the decrease in c-Myc levels antagonized c-Myc–mediated regulation of growth-promoting signaling pathways and glucose metabolism genes (Glut1, HK, LDHA).[32,44] HIF-1α, decreased in si-hVDAC1-TTs, regulates multiple adaptive responses to hypoxia, like, angiogenesis and metabolism, upregulating a number of genes involved in aerobic glycolysis.[45] Thus, decreased expression of c-Myc and HIF-1α in si-hVDAC1-TTs is consistent with the regulation of the cancer cell metabolic circuitry by these TFs. In contrast, p53 expression was increased upon si-hVDAC1 treatment, in accordance with its central role in regulating cell cycle, metabolism and apoptosis,[46] and neural and glioma stem/progenitor cell renewal and differentiation,[21,47] as also observed here. Moreover, U-118MG tumors, which carry mutated p53,[48] responded similarly as U-87MG tumors to si-hVDAC1. The interplay between c-Myc, HIF-1α, and p53 coordinates the regulation of cancer cell metabolism and associated processes via coordinating changes in levels of expression of other TFs and genes that regulate the "transformed phenotype"[22] (Supplementary Table 5).

To conclude, the findings presented here point to VDAC1 as regulating a continuum of cellular functions, from metabolism to cell differentiation. VDAC1 depletion assaults critical functional nodes in the oncogenic network, leading to a multipronged attack on cancer hallmarks, reversing oncogenic properties by reversing cancer-reprogrammed metabolism, thereby inhibiting cell proliferation, tumor growth, EMT, and angiogenesis. VDAC1 depletion also targets GSCs, leading to their differentiation into neuronal-like cells, thus preventing tumor recurrence. By simultaneously attacking all of these processes, si-hVDAC1 represents an innovative and markedly potent therapeutic strategy.

Supplementary Material

Supplementary data are available at *Neuro-Oncology Practice* online.

Funding

This research was supported by Phil and Sima Needleman and Yafa and Ezra Yerucham research funds and by a grant from the Israel Science Foundation (307/13) and from the Israel Cancer Society.

Conflict of interest statement. The authors declare no competing financial interests.

References

1. Bai RY, Staedtke V, Riggins GJ. Molecular targeting of glioblastoma: drug discovery and therapies. *Trends Mol Med*. 2011;17(6):301–312.
2. Singh SK, Hawkins C, Clarke ID, et al. Identification of human brain tumour initiating cells. *Nature*. 2004;432(7015):396–401.
3. Chen J, Li Y, Yu TS, et al. A restricted cell population propagates glioblastoma growth after chemotherapy. *Nature*. 2012;488(7412):522–526.
4. Sottoriva A, Spiteri I, Piccirillo SG, et al. Intratumor heterogeneity in human glioblastoma reflects cancer evolutionary dynamics. *Proc Natl Acad Sci U S A*. 2013;110(10):4009–4014.
5. Hanahan D, Weinberg RA. Hallmarks of cancer: the next generation. *Cell*. 2011;144(5):646–674.
6. Koppenol WH, Bounds PL, Dang CV. Otto Warburg's contributions to current concepts of cancer metabolism. *Nat Rev Cancer*. 2011;11(5):325–337.
7. Gogvadze V, Zhivotovsky B, Orrenius S. The Warburg effect and mitochondrial stability in cancer cells. *Mol Aspects Med*. 2010;31(1):60–74.
8. Cantor JR, Sabatini DM. Cancer cell metabolism: one hallmark, many faces. *Cancer Discov*. 2012;2(10):881–898.
9. Agnihotri S, Zadeh G. Metabolic reprogramming in glioblastoma: the influence of cancer metabolism on epigenetics and unanswered questions. *Neuro Oncol*. 2016;18(2):160–172.
10. Nakano I. Therapeutic potential of targeting glucose metabolism in glioma stem cells. *Expert Opin Ther Targets*. 2014;18(11):1233–1236.
11. Vlashi E, Lagadec C, Vergnes L, et al. Metabolic state of glioma stem cells and nontumorigenic cells. *Proc Natl Acad Sci U S A*. 2011;108(38):16062–16067.
12. Shoshan-Barmatz V, De Pinto V, Zweckstetter M, Raviv Z, Keinan N, Arbel N. VDAC, a multi-functional mitochondrial protein regulating cell life and death. *Mol Aspects Med*. 2010;31(3):227–285.
13. Shoshan-Barmatz V, Ben-Hail D, Admoni L, Krelin Y, Tripathi SS. The mitochondrial voltage-dependent anion channel 1 in tumor cells. *Biochim Biophys Acta*. 2015;1848(10 Pt B):2547–2575.
14. Arif T, Vasilkovsky L, Refaely Y, Konson A, Shoshan-Barmatz V. Silencing VDAC1 Expression by siRNA Inhibits Cancer Cell Proliferation and Tumor Growth In Vivo. *Mol Ther Nucleic Acids*. 2014;3:e159.
15. Feichtinger RG, Weis S, Mayr JA, et al. Alterations of oxidative phosphorylation complexes in astrocytomas. *Glia*. 2014;62(4):514–525.
16. Abu-Hamad S, Sivan S, Shoshan-Barmatz V. The expression level of the voltage-dependent anion channel controls life and death of the cell. *Proc Natl Acad Sci U S A*. 2006;103(15):5787–5792.
17. Koren I, Raviv Z, Shoshan-Barmatz V. Downregulation of voltage-dependent anion channel-1 expression by RNA interference prevents cancer cell growth in vivo. *Cancer Biol Ther*. 2010;9(12):1046–1052.
18. Maldonado EN, Lemasters JJ. Warburg revisited: regulation of mitochondrial metabolism by voltage-dependent anion channels in cancer cells. *J Pharmacol Exp Ther*. 2012;342(3):637–641.
19. Das J, Das S, Paul A, Samadder A, Bhattacharyya SS, Khuda-Bukhsh AR. Assessment of drug delivery and anticancer potentials of nanoparticles-loaded siRNA targeting STAT3 in lung cancer, in vitro and in vivo. *Toxicol Lett*. 2014;225(3):454–466.
20. Pierce AM, Keating AK. Creating anatomically accurate and reproducible intracranial xenografts of human brain tumors. *J Vis Exp*. 2014(91):52017.

21. Xavier JM, Morgado AL, Solá S, Rodrigues CM. Mitochondrial translocation of p53 modulates neuronal fate by preventing differentiation-induced mitochondrial stress. *Antioxid Redox Signal*. 2014;21(7):1009–1024.
22. Yeung SJ, Pan J, Lee MH. Roles of p53, MYC and HIF-1 in regulating glycolysis—the seventh hallmark of cancer. *Cell Mol Life Sci*. 2008;65(24):3981–3999.
23. Mani SA, Guo W, Liao MJ, et al. The epithelial-mesenchymal transition generates cells with properties of stem cells. *Cell*. 2008;133(4):704–715.
24. Barriere G, Fici P, Gallerani G, Fabbri F, Zoli W, Rigaud M. Circulating tumor cells and epithelial, mesenchymal and stemness markers: characterization of cell subpopulations. *Ann Transl Med*. 2014;2(11):109.
25. Head SA, Shi W, Zhao L, et al. Antifungal drug itraconazole targets VDAC1 to modulate the AMPK/mTOR signaling axis in endothelial cells. *Proc Natl Acad Sci U S A*. 2015 29;112(52):E7276–E7285
26. Liu R, Li J, Zhang T, et al. Itraconazole suppresses the growth of glioblastoma through induction of autophagy: involvement of abnormal cholesterol trafficking. *Autophagy*. 2014;10(7):1241–1255.
27. Katoh M, Igarashi M, Fukuda H, Nakagama H, Katoh M. Cancer genetics and genomics of human FOX family genes. *Cancer Lett*. 2013;328(2):198–206.
28. Lunyak VV, Rosenfeld MG. No rest for REST: REST/NRSF regulation of neurogenesis. *Cell*. 2005;121(4):499–501.
29. Cogoi S, Paramasivam M, Membrino A, Yokoyama KK, Xodo LE. The KRAS promoter responds to Myc-associated zinc finger and poly(ADP-ribose) polymerase 1 proteins, which recognize a critical quadruplex-forming GA-element. *J Biol Chem*. 2010;285(29):22003–22016.
30. Wang J, Cheng H, Li X, Lu W, Wang K, Wen T. Regulation of neural stem cell differentiation by transcription factors HNF4-1 and MAZ-1. *Mol Neurobiol*. 2013;47(1):228–240.
31. Anton K, Baehring JM, Mayer T. Glioblastoma multiforme: overview of current treatment and future perspectives. *Hematol Oncol Clin North Am*. 2012;26(4):825–853.
32. Cairns RA, Harris IS, Mak TW. Regulation of cancer cell metabolism. *Nat Rev Cancer*. 2011;11(2):85–95.
33. Moreno-Sánchez R, Marín-Hernández A, Saavedra E, Pardo JP, Ralph SJ, Rodríguez-Enríquez S. Who controls the ATP supply in cancer cells? Biochemistry lessons to understand cancer energy metabolism. *Int J Biochem Cell Biol*. 2014;50:10–23.
34. Zhao Y, Butler EB, Tan M. Targeting cellular metabolism to improve cancer therapeutics. *Cell Death Dis*. 2013;4:e532.
35. Dirks PB. Brain tumor stem cells: the cancer stem cell hypothesis writ large. *Mol Oncol*. 2010;4(5):420–430.
36. Yan X, Ma L, Yi D, et al. A CD133-related gene expression signature identifies an aggressive glioblastoma subtype with excessive mutations. *Proc Natl Acad Sci U S A*. 2011;108(4):1591–1596.
37. Bao S, Wu Q, McLendon RE, et al. Glioma stem cells promote radioresistance by preferential activation of the DNA damage response. *Nature*. 2006;444(7120):756–760.
38. Gomez GG, Volinia S, Croce CM, et al. Suppression of microRNA-9 by mutant EGFR signaling upregulates FOXP1 to enhance glioblastoma tumorigenicity. *Cancer Res*. 2014;74(5):1429–1439.
39. Binello E, Germano IM. Stem cells as therapeutic vehicles for the treatment of high-grade gliomas. *Neuro Oncol*. 2012;14(3):256–265.
40. Zhao Z, Wang L, Di LJ. Compartmentation of metabolites in regulating epigenome of cancer. *Mol Med*. 2016;22.
41. Carrer A, Wellen KE. Metabolism and epigenetics: a link cancer cells exploit. *Curr Opin Biotechnol*. 2015;34:23–29.
42. Justus CR, Sanderlin EJ, Yang LV. Molecular connections between cancer cell metabolism and the tumor microenvironment. *Int J Mol Sci*. 2015;16(5):11055–11086.
43. Perry J, Okamoto M, Guiou M, Shirai K, Errett A, Chakravarti A. Novel therapies in glioblastoma. *Neurol Res Int*. 2012;2012:428565.
44. Miller DM, Thomas SD, Islam A, Muench D, Sedoris K. c-Myc and cancer metabolism. *Clin Cancer Res*. 2012;18(20):5546–5553.
45. Semenza GL. HIF-1 mediates metabolic responses to intratumoral hypoxia and oncogenic mutations. *J Clin Invest*. 2013;123(9):3664–3671.
46. Suzuki K, Matsubara H. Recent advances in p53 research and cancer treatment. *J Biomed Biotechnol*. 2011;2011:978312.
47. Radke J, Bortolussi G, Pagenstecher A. Akt and c-Myc induce stem-cell markers in mature primary p53$^{-/-}$ astrocytes and render these cells gliomagenic in the brain of immunocompetent mice. *PLoS One*. 2013;8(2):e56691.
48. Pan Y, Haines DS. Identification of a tumor-derived p53 mutant with novel transactivating selectivity. *Oncogene*. 2000;19(27):3095–3100.